

# Past Movements-Guided Motion Representation Learning for Human Motion Prediction

Junyu Shi

Baoxuan Wang

junyushi02@gmail.com

wangbxsm@outlook.com

## Abstract

*Human motion prediction based on 3D skeleton is a significant challenge in computer vision, primarily focusing on the effective representation of motion. In this paper, we propose a self-supervised learning framework designed to enhance motion representation. This framework consists of two stages: first, the network is pretrained through the self-reconstruction of past sequences, and the guided reconstruction of future sequences based on past movements. We design a velocity-based mask strategy to focus on the joints with large-scale moving. Subsequently, the pretrained network undergoes finetuning for specific tasks. Self-reconstruction, guided by patterns of past motion, substantially improves the model's ability to represent the spatiotemporal relationships among joints but also captures the latent relationships between past and future sequences. This capability is crucial for motion prediction tasks that solely depend on historical motion data. By employing this straightforward yet effective training paradigm, our method outperforms existing state-of-the-art methods, reducing the average prediction errors by 8.8% across Human3.6M, 3DPW, and AMASS datasets. The code is available at <https://github.com/JunyuShi02/PMG-MRL>.*

## 1. Introduction

3D skeleton-based motion prediction stands as a fundamental task in computer vision, with the objectives of generating consecutive and unseen future motion sequences based on past observations. This technique finds widespread application in domains such as human-computer interaction, autonomous driving, and motion analysis. The key to achieve accurate predictions of future motions lies in effectively modeling motion sequences, particularly the spatiotemporal representation of moving joints. However, due to the inherent properties of human kinematics, joints exhibit complex hierarchical rotational relationships. The motion trajec-

ties of human joints also display a certain degree of randomness. Consequently, effectively capturing the spatiotemporal relationships between joints has perennially posed a challenging problem.

In the early stages, researchers utilized probabilistic models, such as Gaussian processes[38] and nonlinear Markov[19] models, to predict future motion changes based on historical motion sequences. However, these methods are computationally intensive and make strong assumptions about data distribution, which leads to models that are inadequate for real-world prediction scenarios. With the emergence of large-scale datasets[17, 27, 37] and advancements in hardware computing performance, motion prediction tasks started employing deep learning methods based on Recurrent Neural Networks (RNNs)[9, 11, 14, 16, 31]. RNN-based models effectively capture the dependencies between frames in a sequence, but the step-by-step generation approach results in the accumulation of prediction errors. The rise of Graph Neural Networks (GNNs) has brought feed-forward prediction paradigms into the motion prediction[3, 10, 26, 30, 34]. GNNs are well-suited for handling the non-Euclidean distribution properties of joints in spatial dimensions, enabling effective modeling of motion's spatial information. Moreover, methods based on Transformers and Multi Layer Perceptrons (MLPs) have also achieved success in motion prediction tasks[1, 2, 12].

Overall, the mainstream paradigms for 3D skeleton-based motion prediction can be categorized into two main categories: 1) extracting features from historical motion sequences using an encoder and then generating predicted motions by a decoder[11, 20, 23] (as shown in Fig. 1(a)); 2) directly generating predicted motions using a feed-forward network[22, 26, 28] (as shown in Fig. 1(b)). However, the potential of self-supervised learning paradigms based on pretraining has not been sufficiently explored and applied in the field of motion prediction. This limits the ability of models to fully learn the spatiotemporal representations of motion sequences. AuxFormer[41] improves prediction performance by incorporating denoising tasks and

masked feature prediction as auxiliary tasks during training (as shown in Fig. 1(c)). Nevertheless, parallel multi-task prediction encounters challenges such as interference with the main task (future motion prediction) and difficulties in balancing loss weights. Moreover, conducting masked feature prediction directly on the entire sequence lacks an exploration of the relationship between historical and future sequences.

In this paper, we propose a novel motion representation learning method for motion prediction tasks, which comprises two stages: pretraining and finetuning. In the pre-training stage, we apply masking to the joints of future motion sequences and utilize the complete past sequence features to guide the reconstruction of future sequences. This approach not only enhances the model’s reconstruction performance through past sequence features but also allows the model to learn the underlying relationship between historical and future sequences during the pretraining stage. Simultaneously, we also conduct self-reconstruction training based on masking on the past sequences. When applying the mask, we mask the joints with the largest motion changes between adjacent frames (i.e., the set of joints with the highest velocity). These joints serve as the central representation of the primary motion changes. Compared to random masking, this approach avoids learning motion patterns of joints with lower information content. For instance, in the "Eating" action, motion changes are concentrated in the upper limb part, implying that we should focus on the representation learning of the upper limb part (including hand, head, and other joints), rather than the lower limb part with smaller changes.

Motion data contains both temporal and spatial dimensions. Given the outstanding performance of Transformers in temporal modeling tasks and spatial modeling tasks, as well as prior work on using Transformers for motion prediction tasks [1, 32, 41], we employ spatiotemporal Transformers to model motion sequences. Specifically, our method includes two components based on Transformers: the Past Motion Encoder (PME) and the Future Motion Predictor (FMP). The former comprises SpatioTemporal Attention (ST-Attention) modules, while the latter consists of ST-Attention modules and Past Motion Guided Attention (PMG-Attention) modules that fuse historical and future information. By pretraining the parameters of the PME and FMP, and finetuning them for the prediction task, our method significantly outperforms other *state-of-the-art* methods in both long-term and short-term predictions using a straightforward model architecture. It is worth noting that we observe a correlation between the performance improvement of our method and the increase in dataset size, which aligns with the characteristic of self-reconstruction learning requiring large-scale data.

The key contributions of our work can be summarized as

follows:

- We propose a human motion representation learning method based on self-reconstruction pretraining paradigm for motion prediction tasks. This method helps the model learn the intrinsic spatiotemporal structure and features of motion sequences.
- We use past motion features to guide the self-reconstruction of future sequences, which not only improves self-reconstruction performance but also helps the model understand the underlying relationship between past and future sequences in the motion prediction tasks.
- We conduct extensive experiments and demonstrate that our method reduces the average prediction errors by 8.8% compared to *state-of-the-art* methods on the 3DPW, Human3.6M, and AMASS datasets.

## 2. Related Work

### 2.1. 3D Skeleton-based Human Motion Prediction

**RNN-based Methods** Early motion prediction methods employed probability model-based approaches[19, 38]. These methods performed poorly when dealing with complex motions. As RNNs can naturally process sequential data, researchers widely used RNNs and their variants for motion prediction tasks[9, 11, 14, 31]. EDR[9] maps motion sequences to a latent space using a nonlinear encoder and models temporal features using LSTM (Long Short-Term Memory Network). To avoid ambiguity when predicting long-term motions, VAE-LSTM[14] introduces the encoding of control signals into a variational inference framework trained to learn human motion manifolds. United[31] achieves smooth prediction by modeling first-order motion derivatives. To incorporate spatial information modeling, Structure-RNN[18] unfolds the spatiotemporal graph in the temporal dimension and decomposes it into a set of contributing factor components fed into RNN modeling. SkelNet[13], at each time frame, obtains local representations of human structure through special component layer branches.

**Feed-forward Methods** The step-by-step modeling and generation approach of RNNs often leads to the issue of error accumulation. In recent times, many methods have adopted a feed-forward paradigm, utilizing GNN and Transformer models, to generate prediction sequences in a non-autoregressive manner[3, 10, 26, 30, 34]. These approaches leverage graph structures and attention computations that adapt to the non-Euclidean distribution properties of joints in space and time. LTD[28], HisRep[29], SGSN[22], and SPGSN[24] transform motion sequences to the frequency domain, modeling the trajectories of joints. DMGNN[20], MST-GNN[23], MSR-GCN[7], Sybio-GNN[21], and MMotion-Att[30] learn motion pat-

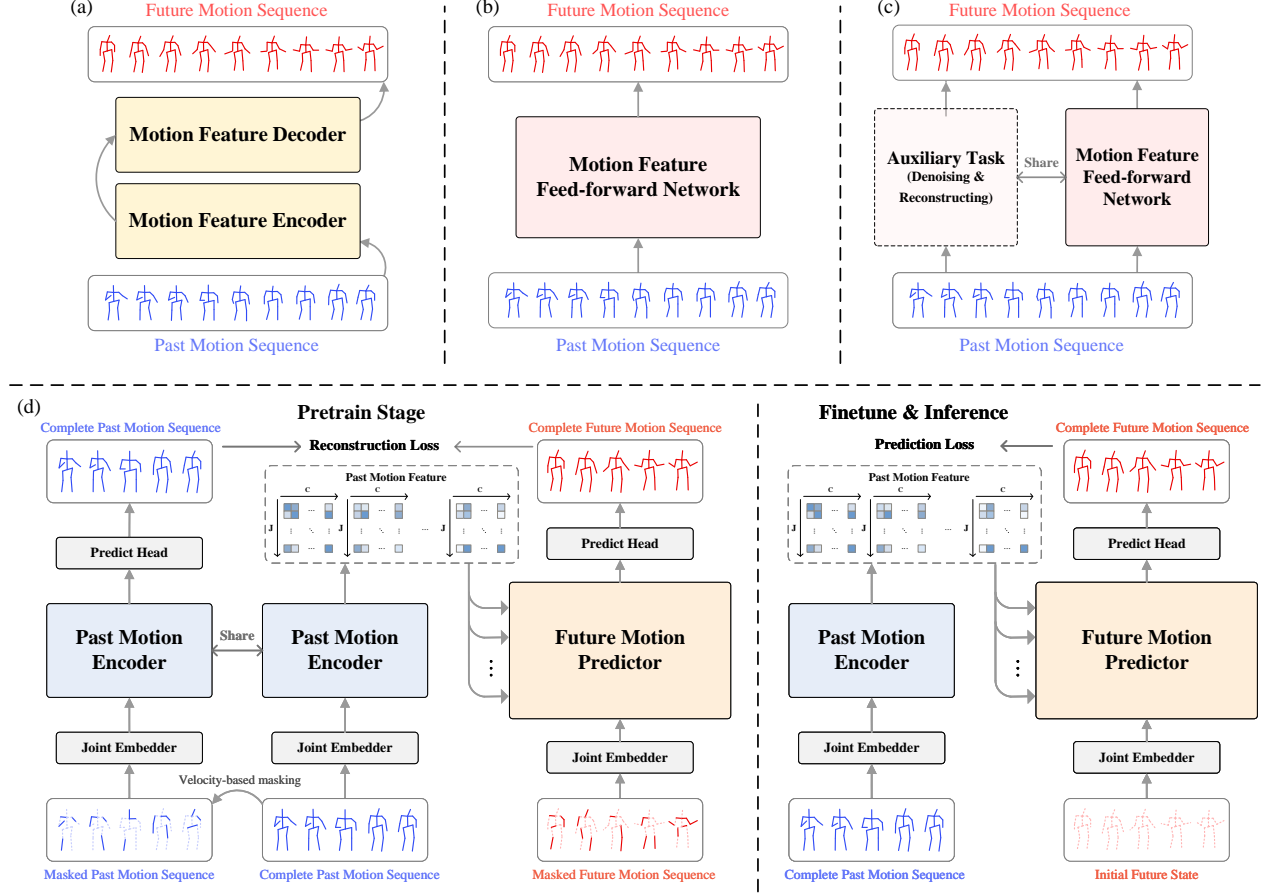


Figure 1. (a) Prediction based on Encoder-Decoder paradigm[20] [23]. (b) Prediction based on Feed-forward paradigm[24] [28]. (c) Enhancing prediction based on auxiliary task[6] [41]. (d) Our Pretrain-Finetune prediction paradigm.

terns at multiple levels by modeling human representations at different scales. DGMGNN[20], MANet[34], DD-GCN[40], and DSTD-GCN[10] model the dynamic characteristics of joints, adapting to the dynamic properties of motion. Transformer-based models utilize self-attention computations, which enhance the model’s capability to capture long-range dependencies between joints[1, 32, 41]. Among them, AuxFormer[41] achieves better results by incorporating denoising and reconstruction tasks to assist the prediction task. In addition, lightweight models based on MLP[2, 12] have also demonstrated success.

## 2.2. Self-supervised Pretraining

Self-supervised pretraining has brought about a revolution in the understanding and generation of language and images. This technique serves as one of the fundamental training methods of Large Language Models (LLMs), which is widely used in BERT[8], RoBERTa[25] and other models. For image processing tasks, recovering masked pixels/tokens is a common self-supervised pretraining method[5, 15]. MAE[15] proves that even when a sub-

stantial portion of image information is masked, the network can reconstruct a complete image based on a limited number of visible features. The self-learning paradigm of autoencoder in MAE is also widely used in multimodal[4], video processing[36], point cloud data processing[42] and other tasks.

## 3. Method

### 3.1. Problem Background

The purpose of 3D skeleton-based human motion prediction is to generate the unseen and consecutive future motion based on past motion patterns. Assume a historical motion sequence consisting of  $T$  frames in the Cartesian coordinate system, denoted as  $\mathbf{X}^P = [\mathbf{x}^1, \mathbf{x}^2, \dots, \mathbf{x}^T] \in \mathbb{R}^{T \times J \times K}$ , where  $J$  represents the number of joints and  $K$  is the feature dimension (the initial value of  $K$  is 3, representing the  $x, y, z$  coordinates). Assume  $\mathbf{X}^F = [\mathbf{x}^1, \mathbf{x}^2, \dots, \mathbf{x}^L] \in \mathbb{R}^{L \times J \times K}$  is the future motion pose of  $L$  frames. Our goal is to design and train a network  $\mathcal{P}(\cdot)$  that takes  $\mathbf{X}^P$  as input and  $\mathbf{X}^F$  as output, i.e.,  $\mathbf{X}^F = \mathcal{P}(\mathbf{X}^P, \pi_\theta)$ , where  $\pi_\theta$  is the

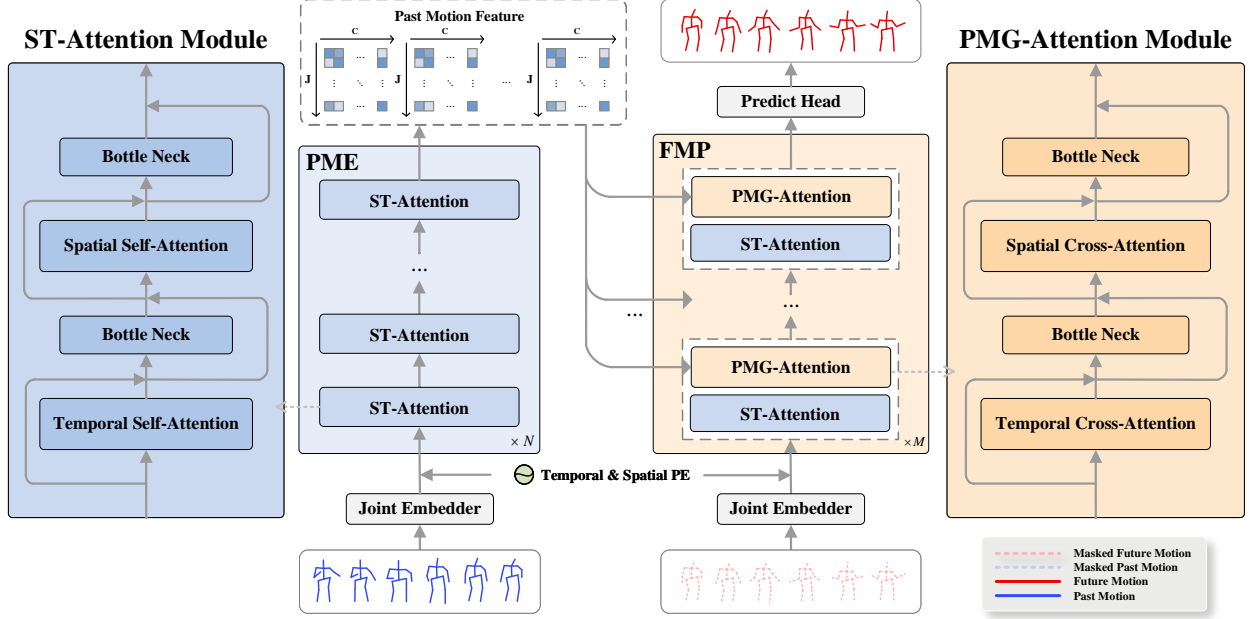


Figure 2. Detail of the model architecture. Our proposed model comprises Past Motion Encoder (PME) and Future Motion Predictor (FMP), where the former consists of  $N \times$  SpatioTemporal Attention (ST-Attention), and the latter consists of  $M$  ST-Attention and Past Motion Guided Attention (PMG-Attention). Here, the finetune stage is taken as an example to show the model structure (the pretrain stage only distinguishes the number of forward propagation of PME and incomplete input sequences).

trainable parameters.

### 3.2. Model Architecture

As shown in Fig. 2, our proposed model consists of a Past Motion Encoder (PME) and a Future Motion Predictor (FMP). The PME aims to extract spatiotemporal features from the past motion sequence. The FMP aims to generate the future motion sequence based on the initial state (which consists of zero-valued inputs in motion prediction tasks) and past motion features.

**Joint Embedder and Predict Head** Given an input sequence  $\mathbf{X}$ , we first use a single linear layer to embed each joint of each frame. To distinguish the spatiotemporal order information of the joints, we add trainable temporal and spatial position encoding to the motion embedding. This process can be represented as:

$$\mathbf{H} = \mathbf{W}\mathbf{X} + \mathbf{b} + \mathbf{P}_t + \mathbf{P}_s \quad (1)$$

where  $\mathbf{W} \in \mathbb{R}^{K \times C}$ ,  $\mathbf{b} \in \mathbb{R}^C$  are the weights and biases of the linear layer, and  $\mathbf{P}_t$ ,  $\mathbf{P}_s$  are the temporal and spatial position encoding, which are randomly initialized and trainable.  $C$  denotes the number of feature channels. For the output of PME and FMP, a linear layer as the Predict Head is applied to obtain the 3D motion sequence.

**Past Motion Encoder (PME)** We design PME to model the features of the past motion sequence. Human motion sequences contain two features: the change of joint position over time and the relationship between joints in space. We use the SpatioTemporal Attention (ST-Attention) to simultaneously model the spatiotemporal information of the joints. Specifically, PME contains  $N$  cascaded ST-Attention modules, where each module first models the sequence dependencies in the temporal dimension and then models the joint relationships in the spatial dimension. Assuming the input to the  $l^{th}$  layer of ST-Transformer is  $\mathbf{H}^l$ , the computation process can be expressed as:

$$\mathbf{H}^{l+1} = \mathcal{F}_{attn}^s(\mathcal{F}_{attn}^t(\mathbf{H}^l)) \quad (2)$$

where  $\mathcal{F}_{attn}^s(\cdot) / \mathcal{F}_{attn}^t(\cdot)$  represents the spatial/temporal multi-head self-attention operation with the bottle neck.

**Future Motion Predictor (FMP)** The purpose of FMP is to generate future motion sequences based on the initial state and the output from PME (i.e., past motion features). FMP comprises two modules: the ST-Attention module for modeling the sequence dependencies within itself and the Past Movement Guided Attention module (PMG-Attention). PMG-Attention applies cross-attention to incorporate past motion features into the current state, which can be mathematically represented as:

$$\mathbf{H}^{l+1} = \mathcal{F}_{c-attn}^s(\mathcal{F}_{c-attn}^t(\mathbf{H}^l, \mathbf{H}^P), \mathbf{H}^P) \quad (3)$$

where  $\mathbf{H}^P$  is the past motion features output by PME.  $\mathbf{H}^l$  is the input of  $l^{th}$  PMG-Attention.  $\mathcal{F}_{c-attn}^s(\cdot) / \mathcal{F}_{c-attn}^t(\cdot)$  represents the spatial/temporal multi-head cross-attention calculation with the bottle neck. We provide more information about the ST-Attention and PMG-Attention in the supplementary materials (Sec. 7).

### 3.3. Past Movement Guided Pretraining

We apply the self-reconstruction pretraining paradigm to help the model learn the spatiotemporal representation of joints in motion sequences (as shown in the left part of Fig. 1(d)), which compromise three steps: 1) past motion reconstruction; 2) past motion encoding; 3) future motion reconstruction. We will introduce each step in the following.

**Past Motion Reconstruction** Given the past motion sequence  $\mathbf{X}^P \in \mathcal{R}^{T \times J \times K}$ , we first calculate the motion velocity of each joint  $\mathbf{V} = \mathbf{X}_{2:T}^P - \mathbf{X}_{1:T-1}^P \in \mathcal{R}^{(T-1) \times J \times K}$ . We find the threshold  $s$  in  $\mathbf{V}$  such that the  $r\%$  of the values in  $\mathbf{V}$  are greater than the threshold  $s$ . The mask of the past motion sequence  $\mathbf{M}^P$  can be mathematically expressed as:

$$\mathbf{M}^{P,(i,j)} = \begin{cases} 1 & , \mathbf{V}^{(i,j)} \geq s \\ 0 & , \mathbf{V}^{(i,j)} < s \end{cases} \quad (4)$$

The masked past motion sequence can be computed by  $\mathbf{X}_{masked}^P = \mathbf{X}^P \times \mathbf{M}^P$ . Then, the joint embedders are applied to obtain the masked motion embeds  $\mathbf{X}_{emb}^P$ . Noting that we incorporate the trainable temporal and spatial position encoding into the motion embeds to learn the temporal order and spatial relationships of joints. Finally, we calculate the reconstructed motion sequence  $\mathbf{X}_{rec}^P = \mathcal{F}_{PH}(\mathcal{F}_{PME}(\mathbf{X}_{emb}^P))$ , where  $\mathcal{F}_{PH}(\cdot)$  and  $\mathcal{F}_{PME}(\cdot)$  are Predict Head and Position Motion Encoder.

**Past Motion Encoding** This step aims to compute the features of complete past motion, which will be used to guide the future motion reconstruction and integrate the hidden relationship between the past sequence and the future sequence into the network. Given the complete input sequence  $\mathbf{X}^P$ , we first apply joint embedder to obtain the motion embeds  $\mathbf{X}_{emb}^P$ . Then, the past motion features can be computed by  $\mathbf{H}^P = \mathcal{F}_{PME}(\mathbf{X}_{emb}^P)$ .

**Future Motion Reconstruction** Given the future motion sequence  $\mathbf{X}^F \in \mathcal{R}^{L \times J \times K}$ , we first use the same method for masking and embedding the future motion sequence as for processing the past motion sequence. The masked future motion embeds, denoted as  $\mathbf{X}_{emb}^F$  and the complete past

motion features  $\mathbf{H}^P$  are the input of FMP. In the PMG-Attention of FMP, past motion features guide the reconstruction of masked future motion through cross-attention mechanism. Finally, the reconstructed motion sequence can be expressed as:  $\mathbf{X}_{rec}^F = \mathcal{F}_{PH}(\mathcal{F}_{FMP}(\mathbf{X}_{emb}^F, \mathbf{H}^P))$ .

### 3.4. Fine-tuning for Motion Prediction

In the finetune phase, we use the complete past motion sequence as input to the PME to get past motion features (as shown in the right part of Fig. 1(d)). In FMP, we use the initial state initialized with the value of 0 (but retain the position encoding) as input, and output the complete future sequence guided by the past motion features. Given the past motion sequence  $\mathbf{X}^P$ , this process can be represented as:

$$\mathbf{H}^P = \mathcal{F}_{JE}(\mathcal{F}_{PME}(\mathbf{X}^P)) \quad (5)$$

$$\mathbf{H}^F = \mathcal{F}_{JE}(\mathcal{F}_{FMP}(\mathbf{H}_0^F, \mathbf{H}^P)) \quad (6)$$

$$\mathbf{X}^F = \mathcal{F}_{PH}(\mathbf{H}^F) \quad (7)$$

where  $\mathbf{H}_0^F$  is the initial state initialized with the value of 0.  $\mathcal{F}_{JE}$  represents the joint embedder.

### 3.5. Loss Function

**Loss Function of Pretrain Stage** Pretrain stage performs past sequence reconstruction and future sequence reconstruction. Given the past and future reconstructed results  $\hat{\mathbf{X}}_{rec}^P$  and  $\hat{\mathbf{X}}_{rec}^F$ , and the corresponding ground-truth (i.e. complete sequence)  $\mathbf{X}_{rec}^P$  and  $\mathbf{X}_{rec}^F$ , the loss function can be represented as follow:

$$\begin{aligned} \mathcal{L}_{pretrain} = & \frac{1}{TJ} \sum_{t=1}^T \sum_{j=1}^J \|\mathbf{X}_{rec}^{P,(t,j)} - \hat{\mathbf{X}}_{rec}^{P,(t,j)}\|_F^2 \\ & + \frac{\alpha}{LJ} \sum_{l=1}^L \sum_{j=1}^J \|\mathbf{X}_{rec}^{F,(l,j)} - \hat{\mathbf{X}}_{rec}^{F,(l,j)}\|_F^2 \end{aligned} \quad (8)$$

where  $\alpha$  is the hyperparameter to balance the loss weight.

**Loss Function of finetune Stage** For finetune stage, given the predicted sequence  $\hat{\mathbf{X}}$  and the ground-truth  $\mathbf{X}$ , the loss function can be defined as:

$$\mathcal{L}_{finetune} = \frac{1}{LJ} \sum_{l=1}^L \sum_{j=1}^J \|\mathbf{X}_j^l - \hat{\mathbf{X}}_j^l\|_F^2 \quad (9)$$

## 4. Experiments

### 4.1. Dataset

**Human3.6M** Human3.6M[17] is a large-scale, accurately annotated 3D human pose dataset that captures the

Table 1. Comparisons of MPJPEs between our proposed method with other *state-of-the-art* methods for short-term prediction on Human3.6. We show the results of detailed actions such as walking and eating. The best results are highlighted in bold, and the second best results are underlined.

Motion	Walking				Eating				Smoking				Discussion			
Milliseconds	80	160	320	400	80	160	320	400	80	160	320	400	80	160	320	400
DMGNN[20]	17.3	30.7	54.6	65.2	11.0	21.4	36.2	43.9	9.0	17.6	32.1	40.3	17.3	34.8	61.0	69.8
MSR[7]	12.2	22.7	38.6	45.2	8.4	17.1	33.0	40.4	8.0	16.3	31.3	38.2	12.0	26.8	57.1	69.7
Mixer[2]	12.0	23.0	42.4	51.3	7.8	16.5	34.3	43.0	7.4	15.2	30.3	37.6	10.7	25.0	56.9	71.1
PGBIG[26]	10.2	19.8	34.5	40.3	7.0	15.1	30.6	38.1	6.6	14.1	28.2	34.7	10.0	23.8	53.6	66.7
SPGSN[24]	10.1	19.4	34.8	41.5	7.1	14.8	30.5	37.9	6.7	13.8	28.0	34.6	10.4	23.8	53.6	67.1
siMLPe[12]	11.9	19.3	31.9	<u>36.9</u>	10.2	16.5	30.7	37.3	10.4	16.4	29.7	35.9	12.7	25.3	55.1	68.1
DSTD-GC[10]	11.1	22.4	38.8	45.2	7.0	15.5	31.7	39.2	6.6	14.8	29.8	36.7	10.0	24.4	54.5	67.4
AuxFormer[41]	8.9	<u>16.9</u>	<b>30.1</b>	<b>36.1</b>	<u>6.4</u>	<u>14.0</u>	<b>28.8</b>	<b>35.9</b>	<u>5.7</u>	<u>11.4</u>	<u>22.1</u>	<u>27.9</u>	<u>8.6</u>	<u>18.8</u>	<u>38.8</u>	<b>49.2</b>
CIST-GCN[33]	11.8	23.4	40.5	46.5	6.7	14.8	29.8	<u>36.8</u>	7.3	15.6	31.0	38.0	10.2	23.7	52.3	65.3
Ours	<b>8.6</b>	<b>16.5</b>	<u>31.2</u>	37.7	<b>6.1</b>	<b>13.7</b>	<u>29.3</u>	<u>36.8</u>	<b>5.3</b>	<b>10.3</b>	<b>19.7</b>	<b>25.2</b>	<b>7.7</b>	<b>16.3</b>	<b>31.7</b>	<b>40.9</b>
Motion	Direction				Greeting				Phoning				Posing			
Milliseconds	80	160	320	400	80	160	320	400	80	160	320	400	80	160	320	400
DMGNN[20]	13.1	24.6	64.7	81.9	23.3	50.3	107.3	132.1	12.5	25.8	48.1	58.3	15.3	29.3	71.5	96.7
MSR[7]	8.6	19.7	43.3	53.8	16.5	37.0	77.3	93.4	10.1	20.7	41.5	51.3	12.8	29.4	67.0	85.0
Mixer[2]	7.5	18.4	43.9	55.3	16.4	37.1	80.2	98.2	9.1	19.5	42.4	53.6	11.5	27.0	64.9	83.5
PGBIG[26]	7.2	17.6	40.9	51.5	15.2	34.1	71.6	87.1	8.3	18.3	38.7	48.4	10.7	25.7	60.0	76.6
SPGSN[24]	7.4	17.2	<u>40.0</u>	<b>50.3</b>	14.6	32.6	70.6	86.4	8.7	18.3	38.7	48.5	10.7	25.3	59.9	76.5
siMLPe[12]	11.0	19.4	41.6	52.1	16.2	33.7	70.9	86.3	11.9	20.3	39.7	48.9	13.9	27.3	62.0	78.6
DSTD-GC[10]	6.9	17.4	40.1	51.7	14.3	33.5	72.2	87.3	8.5	19.2	40.3	49.9	10.1	25.4	60.6	77.3
AuxFormer[41]	<u>6.8</u>	<u>17.0</u>	40.3	51.6	<u>13.5</u>	31.3	69.2	85.4	<u>7.9</u>	<u>17.3</u>	<b>37.4</b>	<b>47.2</b>	<u>8.8</u>	<u>19.1</u>	<u>39.2</u>	<b>51.0</b>
CIST-GCN[33]	7.3	18.1	43.6	55.3	13.7	<u>31.0</u>	<u>65.7</u>	<u>79.9</u>	8.6	18.5	39.3	49.6	9.6	23.7	57.7	75.0
Ours	<b>6.3</b>	<b>15.8</b>	<b>39.8</b>	<u>51.4</u>	<b>10.8</b>	<b>26.4</b>	<b>62.7</b>	<b>79.8</b>	<b>7.5</b>	<b>17.1</b>	37.9	<u>48.0</u>	<b>8.2</b>	<b>16.9</b>	<b>32.8</b>	<b>43.5</b>

Table 2. Comparisons of MPJPEs between our proposed method with other *state-of-the-art* methods for short- and long- term prediction on Human3.6M. We show the average result of all actions. The best results are highlighted in bold.

Motion	Average						Param(M)
Milliseconds	80	160	320	400	560	1000	-
DMGNN[20]	17.0	33.6	65.9	79.7	103.0	137.2	4.82
MSR[7]	12.1	25.6	51.6	62.9	81.1	114.2	6.30
Mixer[2]	11.1	24.0	51.5	64.0	83.5	116.5	0.03
PGBIG[26]	10.3	22.7	47.4	58.5	76.9	110.3	1.80
SPGSN[24]	10.4	22.3	47.1	58.3	77.1	108.8	5.66
siMLPe[12]	13.4	23.7	47.4	58.0	77.9	111.7	0.14
DSTD-GC[10]	10.4	23.3	48.8	59.8	77.8	111.0	0.18
AuxFormer[41]	9.5	20.6	43.4	54.1	75.3	107.0	1.00
CIST-GCN[33]	10.5	23.2	47.9	59.0	77.2	110.3	0.35
GCNext [39]	9.3	21.5	45.5	56.4	74.7	108.7	-
Ours	<b>8.8</b>	<b>19.3</b>	<b>41.1</b>	<b>51.8</b>	<b>70.0</b>	<b>101.5</b>	1.66

motions of 11 professional actors in daily life scenarios using motion capture technology, totaling over 3.6 million pose instances. Following previous works[24, 26], only 22 joints are used, focusing on those that exhibit significant movement, and all sequences are down-sampled to 25 fps.

**The 3D Poses in the Wild (3DPW)** 3DPW[37] stands out as a pioneering dataset in motion related tasks, primarily due to its focus on capturing human motion in natural settings outside of the typical laboratory environment. This dataset provides a rich collection of video sequences captured at a frame rate of 30 frames per second, which includes diverse activities such as 'Walking', 'Running', and interacting with various objects.

**The Archive of Motion Capture as Surface Shapes (AMASS)** AMASS[27] consolidates 15 existing motion capture datasets into a single, standardized framework. By converting these diverse datasets into a common representation, AMASS provides over 40 hours of meticulously annotated motion data. Following the previous works[34, 40], we discarded the detailed joints of the hand and sampled the sequence to 24fps.

## 4.2. Experimental Settings

For the PME and the FMP, the number of modules (denoted as  $N, M$ ) are both set to 3. The number of feature channels remains consistent at 128 throughout the network architecture. In the attention calculation, we employed 8 heads, with each head comprising 32 feature channels. During the pretraining phase, the loss weight (denoted as  $\alpha$ ) is set to 1,

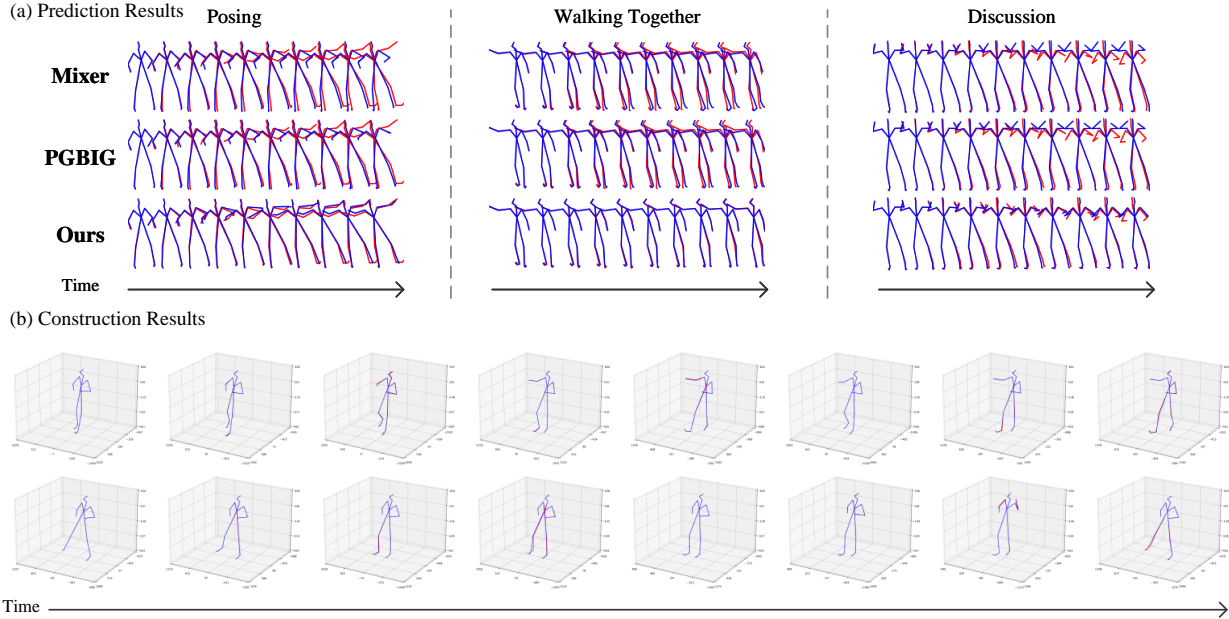


Figure 3. Visualization results of short-term prediction (a) and reconstruction (b). The blue lines represent predicted/reconstructed motions, and the red lines represent ground-truths. We map the results to 2D space for display.

indicating an equal contribution of loss from both past and future sequence reconstruction. We provide more implementation details in the supplementary materials (Sec. 8).

### 4.3. Comparison to State-of-the-art Methods

We compare our method with the recent *state-of-the-art* methods, including DMGNN (CVPR’20)[1, 2, 7, 10, 12, 20, 24, 26, 30, 33, 39–41]. To ensure fair comparisons, we re-evaluated some methods on the entire test set to align the testing standard using their official pretrained models, or retrain the model (Only for the cases where the official pre-training model is not provided) using their default hyperparameters on the Human3.6M.

**Comparisons on Human3.6M** We use MPJPE (Mean Per Joint Position Error) as the evaluation metric, which is widely used in motion prediction tasks[24, 26, 41]. Tab. 1 shows the quantitative comparisons of short-term motion prediction on Human3.6M dataset, which aims to predict the poses within 400 milliseconds. Detailed actions are listed. As can be seen, our method outperforms the others on most actions, especially the "Smoking", "Greeting", and "Posing". Tab. 2 displays the average results of short - and long-term predictions for all actions on Human3.6M. Our approach effectively reduces prediction errors by 5.4%/10.2%/9.7%/8.2%/6.3%/6.6% at 80ms/160ms/320ms/400ms/560ms/1000ms.

Table 3. Comparisons of MPJPEs between our proposed method with other *state-of-the-art* methods for both short-term and long-term prediction on AMASS. The best results are highlighted in bold.

Milliseconds	80	160	320	400	560	720	880	1000
LTD-10-10[28]	10.3	19.3	36.6	44.6	61.5	75.9	86.2	91.2
LTD-10-25[28]	11.0	20.7	37.8	45.3	57.2	65.7	71.3	75.2
HisRep[29]	11.3	20.7	35.7	42.0	51.7	58.6	63.4	67.2
Mao W, et al.[30]	11.0	20.3	35.0	41.2	50.7	57.4	61.9	65.8
siMLPe[12]	10.8	19.6	34.3	40.5	50.5	57.3	62.4	65.7
DD-GCN[40]	10.4	19.1	33.6	39.8	49.3	56.5	61.3	64.6
<b>Ours</b>	<b>8.6</b>	<b>15.3</b>	<b>27.7</b>	<b>33.2</b>	<b>42.0</b>	<b>48.3</b>	<b>53.0</b>	<b>56.0</b>

**Comparisons on AMASS** Tab. 3 shows the comparisons on AMASS dataset. Our method achieves a reduction in prediction errors of 17.3%/19.9%/17.6%/16.6%/14.8%/14.5%/13.5%/13.3% at 80ms/160ms/320ms/400ms/560ms/720ms/880ms/1000ms. We found that our method exhibits the most significant improvement on this dataset. This can be attributed to the larger data size of AMASS compared to Human3.6M and 3DPW. The self-reconstruction pretraining enables our model to learn a more comprehensive representation of motion on such a large dataset.

**Comparisons on 3DPW** The 3DPW dataset comprises data collected from outside the laboratory setting, which are widely used to verify the power of the model in real scenar-

Table 4. Comparisons of MPJPEs between our proposed method with other *state-of-the-art* methods for short- and long-term prediction on 3DPW. The best results are highlighted in bold.

Milliseconds	Average MPJPE					
	100	200	400	600	800	1000
DMGNN[20]	17.80	37.11	70.38	94.12	109.67	123.93
HisRep[29]	15.88	35.14	66.82	93.55	107.63	114.75
MSR-GCN[7]	15.70	33.48	65.02	93.81	108.15	116.31
STGCN[35]	18.32	37.79	67.51	92.75	106.65	112.22
PGBIG[26]	17.66	35.32	67.83	89.60	102.59	109.41
SPGNN[24]	15.39	32.91	64.54	91.62	103.98	111.05
AuxFormer[41]	14.21	30.04	58.50	89.45	100.78	107.45
Ours	<b>13.85</b>	<b>29.11</b>	<b>57.06</b>	<b>87.35</b>	<b>97.93</b>	<b>103.37</b>

ios. As shown in Tab. 4, our approach performed best across all frames, showcasing its robustness in handling complex interactive scenarios.

Table 5. Comparison of Motion Classification Using Network-Output Features

	w/o Network	AuxFormer[41]	Ours
Accuracy	25.6%	80.8%	95.0%

**Representation Capability** To validate the representation learning capability of our proposed method, we first extract motion features from the outputs of the trained model (outputs from the penultimate layer). Subsequently, we train a simple linear classifier to classify these features. As shown in Tab. 5, our method significantly improves classification accuracy compared to methods that do not involve feature extraction via neural networks and AuxFormer[41].

#### 4.4. Visualization of Prediction and Reconstruction

Fig. 3 (a) presents the visualization of prediction results. We conducted comparisons with PGBIG[26] and Mixer[2] on challenging samples. In the 'Posing' and 'Discussion' actions, our model successfully captures significant upward/downward movements of the arms. This can be attributed to the utilization of past motion guidance, which enables the model to comprehend the influence of previous motion patterns on future sequences. We also provide reconstruction results with a mask rate of 75% in Fig. 3 (b). Similar to the property of mask-based pretraining[15], even with a high mask rate of 75% for joints, the model can still accurately reconstruct the exact location of them.

#### 5. Ablation Study

In this section, we explore the impact of components of our network, including the mask strategy, pretraining paradigm.

Table 6. Impact of mask strategy and pretraining paradigm.  $r$  is the mask rate. 'denoise' means we conduct self-supervised pre-training by denoising.

ID		80ms	160ms	320ms	400ms
A	random mask	9.0	19.7	42.4	52.8
B	$r = 0\%$	9.6	21.9	46.2	56.8
C	$r = 25\%$	9.3	20.2	42.9	53.7
D	$r = 50\%$	9.1	20.0	42.3	52.6
E	denoise	9.2	20.4	42.9	53.8
F	complete ( $r = 75\%$ )	8.8	19.3	41.1	51.8

We provide studies on model architecture in the supplementary materials. All experiments were carried out on the Human3.6M dataset.

**Mask Strategy** Tab. 6 presents the results of two cases: A, without utilizing the velocity-based mask strategy (i.e. randomly mask 75% of the joints), and F, which represents the complete model. It can be seen that using the velocity-based mask reduced the average prediction errors by 2.3%. Tab. 6 also shows the comparisons of different mask rates (ranging from 0% to 75%), represented by B, C, D, F. The high mask rate facilitates the model to learn the space-time representation during the self-reconstruction process.

**Effects of Pretraining Paradigm** We show the results of pretraining the model by denoising in Tab. 6 E. Compared with the self-reconstruction, denoising pretraining method lacks the exploration of the spatiotemporal relationship between joints.

## 6. Conclusion

In this paper, we propose a novel motion prediction paradigm, which consists two stages: 1) Past motion guided future motion self-reconstruction for learning the spatio-temporal representation of human joints (i.e. pre-train stage). 2) Train the network for the motion prediction task (i.e. finetune stage). Despite the simplicity of the model structure, our approach achieves the best results on three representative datasets and is highly extensible.

## References

- [1] Emre Aksan, Manuel Kaufmann, Peng Cao, and Otmar Hilliges. A spatio-temporal transformer for 3d human motion prediction. In *2021 International Conference on 3D Vision (3DV)*, pages 565–574. IEEE, 2021. [1](#), [2](#), [3](#), [7](#)
- [2] Arij Bouazizi, Adrian Holzbock, Ulrich Kressel, Klaus Dietmayer, and Vasileios Belagiannis. Motionmixer: mlp-based 3d human body pose forecasting. *arXiv preprint arXiv:2207.00499*, 2022. [1](#), [3](#), [6](#), [7](#), [8](#), [2](#)

[3] Yujun Cai, Lin Huang, Yiwei Wang, Tat-Jen Cham, Jianfei Cai, Junsong Yuan, Jun Liu, Xu Yang, Yiheng Zhu, Xiaohui Shen, et al. Learning progressive joint propagation for human motion prediction. In *Computer Vision–ECCV 2020: 16th European Conference, Glasgow, UK, August 23–28, 2020, Proceedings, Part VII 16*, pages 226–242. Springer, 2020. 1, 2

[4] Anthony Chen, Kevin Zhang, Renrui Zhang, Zihan Wang, Yuheng Lu, Yandong Guo, and Shanghang Zhang. Pimae: Point cloud and image interactive masked autoencoders for 3d object detection. In *Proceedings of the IEEE/CVF Conference on Computer Vision and Pattern Recognition*, pages 5291–5301, 2023. 3

[5] Xiaokang Chen, Mingyu Ding, Xiaodi Wang, Ying Xin, Shentong Mo, Yunhao Wang, Shumin Han, Ping Luo, Gang Zeng, and Jingdong Wang. Context autoencoder for self-supervised representation learning. *International Journal of Computer Vision*, 132(1):208–223, 2024. 3

[6] Qiongjie Cui, Huaijiang Sun, Jianfeng Lu, Bin Li, and Weiqing Li. Meta-auxiliary learning for adaptive human pose prediction. In *Proceedings of the AAAI Conference on Artificial Intelligence*, pages 6166–6174, 2023. 3

[7] Lingwei Dang, Yongwei Nie, Chengjiang Long, Qing Zhang, and Guiqing Li. Msr-gcn: Multi-scale residual graph convolution networks for human motion prediction. In *Proceedings of the IEEE/CVF International Conference on Computer Vision*, pages 11467–11476, 2021. 2, 6, 7, 8

[8] Jacob Devlin, Ming-Wei Chang, Kenton Lee, and Kristina Toutanova. Bert: Pre-training of deep bidirectional transformers for language understanding. *arXiv preprint arXiv:1810.04805*, 2018. 3

[9] Katerina Fragkiadaki, Sergey Levine, Panna Felsen, and Jitendra Malik. Recurrent network models for human dynamics. In *Proceedings of the IEEE international conference on computer vision*, pages 4346–4354, 2015. 1, 2

[10] Jiajun Fu, Fuxing Yang, Yonghao Dang, Xiaoli Liu, and Jian-qin Yin. Learning constrained dynamic correlations in spatiotemporal graphs for motion prediction. *IEEE Transactions on Neural Networks and Learning Systems*, 2023. 1, 2, 3, 6, 7

[11] Partha Ghosh, Jie Song, Emre Aksan, and Otmar Hilliges. Learning human motion models for long-term predictions. In *2017 International Conference on 3D Vision (3DV)*, pages 458–466. IEEE, 2017. 1, 2

[12] Wen Guo, Yuming Du, Xi Shen, Vincent Lepetit, Xavier Alameda-Pineda, and Francesc Moreno-Noguer. Back to mlp: A simple baseline for human motion prediction. In *Proceedings of the IEEE/CVF Winter Conference on Applications of Computer Vision*, pages 4809–4819, 2023. 1, 3, 6, 7, 2

[13] Xiao Guo and Jongmoo Choi. Human motion prediction via learning local structure representations and temporal dependencies. In *Proceedings of the AAAI Conference on Artificial Intelligence*, pages 2580–2587, 2019. 2

[14] Ihsanul Habibie, Daniel Holden, Jonathan Schwarz, Joe Yearsley, and Taku Komura. A recurrent variational autoencoder for human motion synthesis. In *Proceedings of the British Machine Vision Conference (BMVC)*, 2017. 1, 2

[15] Kaiming He, Xinlei Chen, Saining Xie, Yanghao Li, Piotr Dollár, and Ross Girshick. Masked autoencoders are scalable vision learners. In *Proceedings of the IEEE/CVF conference on computer vision and pattern recognition*, pages 16000–16009, 2022. 3, 8

[16] Junfeng Hu, Zhencheng Fan, Jun Liao, and Li Liu. Predicting long-term skeletal motions by a spatio-temporal hierarchical recurrent network. In *Proceedings of the 24th European Conference on Artificial Intelligence*, pages 2720–2727, 2020. 1

[17] Catalin Ionescu, Dragos Papava, Vlad Olaru, and Cristian Sminchisescu. Human3. 6m: Large scale datasets and predictive methods for 3d human sensing in natural environments. *IEEE transactions on pattern analysis and machine intelligence*, 36(7):1325–1339, 2013. 1, 5

[18] Ashesh Jain, Amir R Zamir, Silvio Savarese, and Ashutosh Saxena. Structural-rnn: Deep learning on spatio-temporal graphs. In *Proceedings of the ieee conference on computer vision and pattern recognition*, pages 5308–5317, 2016. 2

[19] Andreas M Lehrmann, Peter V Gehler, and Sebastian Nowozin. Efficient nonlinear markov models for human motion. In *Proceedings of the IEEE Conference on Computer Vision and Pattern Recognition*, pages 1314–1321, 2014. 1, 2

[20] Maosen Li, Siheng Chen, Yangheng Zhao, Ya Zhang, Yanfeng Wang, and Qi Tian. Dynamic multiscale graph neural networks for 3d skeleton based human motion prediction. In *Proceedings of the IEEE/CVF conference on computer vision and pattern recognition*, pages 214–223, 2020. 1, 2, 3, 6, 7, 8

[21] Maosen Li, Siheng Chen, Xu Chen, Ya Zhang, Yanfeng Wang, and Qi Tian. Symbiotic graph neural networks for 3d skeleton-based human action recognition and motion prediction. *IEEE Transactions on Pattern Analysis and Machine Intelligence*, 44(6):3316–3333, 2021. 2

[22] Maosen Li, Siheng Chen, Zihui Liu, Zijing Zhang, Lingxi Xie, Qi Tian, and Ya Zhang. Skeleton graph scattering networks for 3d skeleton-based human motion prediction. In *Proceedings of the IEEE/CVF international conference on computer vision*, pages 854–864, 2021. 1, 2

[23] Maosen Li, Siheng Chen, Yangheng Zhao, Ya Zhang, Yanfeng Wang, and Qi Tian. Multiscale spatio-temporal graph neural networks for 3d skeleton-based motion prediction. *IEEE Transactions on Image Processing*, 30:7760–7775, 2021. 1, 2, 3

[24] Maosen Li, Siheng Chen, Zijing Zhang, Lingxi Xie, Qi Tian, and Ya Zhang. Skeleton-parted graph scattering networks for 3d human motion prediction. In *Computer Vision–ECCV 2022: 17th European Conference, Tel Aviv, Israel, October 23–27, 2022, Proceedings, Part VI*, pages 18–36. Springer, 2022. 2, 3, 6, 7, 8

[25] Yinhan Liu, Myle Ott, Naman Goyal, Jingfei Du, Mandar Joshi, Danqi Chen, Omer Levy, Mike Lewis, Luke Zettlemoyer, and Veselin Stoyanov. Roberta: A robustly optimized bert pretraining approach. *arXiv preprint arXiv:1907.11692*, 2019. 3

[26] Tiezheng Ma, Yongwei Nie, Chengjiang Long, Qing Zhang, and Guiqing Li. Progressively generating better initial

guesses towards next stages for high-quality human motion prediction. In *Proceedings of the IEEE/CVF Conference on Computer Vision and Pattern Recognition*, pages 6437–6446, 2022. 1, 2, 6, 7, 8

[27] Naureen Mahmood, Nima Ghorbani, Nikolaus F Troje, Gerard Pons-Moll, and Michael J Black. Amass: Archive of motion capture as surface shapes. In *Proceedings of the IEEE/CVF international conference on computer vision*, pages 5442–5451, 2019. 1, 6

[28] Wei Mao, Miaomiao Liu, Mathieu Salzmann, and Hongdong Li. Learning trajectory dependencies for human motion prediction. In *Proceedings of the IEEE/CVF International Conference on Computer Vision*, pages 9489–9497, 2019. 1, 2, 3, 7

[29] Wei Mao, Miaomiao Liu, and Mathieu Salzmann. History repeats itself: Human motion prediction via motion attention. In *Computer Vision–ECCV 2020: 16th European Conference, Glasgow, UK, August 23–28, 2020, Proceedings, Part XIV 16*, pages 474–489. Springer, 2020. 2, 7, 8

[30] Wei Mao, Miaomiao Liu, Mathieu Salzmann, and Hongdong Li. Multi-level motion attention for human motion prediction. *International journal of computer vision*, 129(9):2513–2535, 2021. 1, 2, 7

[31] Julieta Martinez, Michael J Black, and Javier Romero. On human motion prediction using recurrent neural networks. In *Proceedings of the IEEE conference on computer vision and pattern recognition*, pages 2891–2900, 2017. 1, 2

[32] Angel Martínez-González, Michael Villamizar, and Jean-Marc Odobez. Pose transformers (potr): Human motion prediction with non-autoregressive transformers. In *Proceedings of the IEEE/CVF International Conference on Computer Vision*, pages 2276–2284, 2021. 2, 3

[33] Edgar Medina, Leyong Loh, Namrata Gurung, Kyung Hun Oh, and Niels Heller. Context-based interpretable spatio-temporal graph convolutional network for human motion forecasting. In *Proceedings of the IEEE/CVF Winter Conference on Applications of Computer Vision*, pages 3232–3241, 2024. 6, 7, 2

[34] Junyu Shi, Jianqi Zhong, and Wenming Cao. Multi-semantics aggregation network based on the dynamic-attention mechanism for 3d human motion prediction. *IEEE Transactions on Multimedia*, 26:5194–5206, 2024. 1, 2, 3, 6

[35] Theodoros Sofianos, Alessio Sampieri, Luca Franco, and Fabio Galasso. Space-time-separable graph convolutional network for pose forecasting. In *Proceedings of the IEEE/CVF International Conference on Computer Vision*, pages 11209–11218, 2021. 8

[36] Zhan Tong, Yibing Song, Jue Wang, and Limin Wang. Videomae: Masked autoencoders are data-efficient learners for self-supervised video pre-training. *Advances in neural information processing systems*, 35:10078–10093, 2022. 3

[37] Timo Von Marcard, Roberto Henschel, Michael J Black, Bodo Rosenhahn, and Gerard Pons-Moll. Recovering accurate 3d human pose in the wild using imus and a moving camera. In *Proceedings of the European conference on computer vision (ECCV)*, pages 601–617, 2018. 1, 6

[38] Jack M Wang, David J Fleet, and Aaron Hertzmann. Gaussian process dynamical models for human motion. *IEEE transactions on pattern analysis and machine intelligence*, 30(2):283–298, 2007. 1, 2

[39] Xinshun Wang, Qiongjie Cui, Chen Chen, and Mengyuan Liu. Gcnext: Towards the unity of graph convolutions for human motion prediction. In *Proceedings of the AAAI Conference on Artificial Intelligence*, pages 5642–5650, 2024. 6, 7

[40] Xinshun Wang, Wanying Zhang, Can Wang, Yuan Gao, and Mengyuan Liu. Dynamic dense graph convolutional network for skeleton-based human motion prediction. *IEEE Transactions on Image Processing*, 33:1–15, 2024. 3, 6, 7

[41] Chenxin Xu, Robby T Tan, Yuhong Tan, Siheng Chen, Xinchao Wang, and Yanfeng Wang. Auxiliary tasks benefit 3d skeleton-based human motion prediction. In *Proceedings of the IEEE/CVF International Conference on Computer Vision*, pages 9509–9520, 2023. 1, 2, 3, 6, 7, 8

[42] Renrui Zhang, Liuhui Wang, Yu Qiao, Peng Gao, and Hongsheng Li. Learning 3d representations from 2d pre-trained models via image-to-point masked autoencoders. In *Proceedings of the IEEE/CVF Conference on Computer Vision and Pattern Recognition*, pages 21769–21780, 2023. 3

# Past Movements-Guided Motion Representation Learning for Human Motion Prediction

## Supplementary Material

In this supplementary material, we provide more information that could not be included in the main manuscript because of space limit, including explanation of ST-Attention and PMG-Attention (in Sec. 7), implementation details (in Sec. 8), complete results for testing on Human3.6M dataset (in Sec. 9), ablation study on model architecture (in Sec. 10), and visualization of feature map (in Sec. 11).

### 7. Detailed Explanation of ST-Attention and PMG-Attention

In our model architecture for human motion prediction, both the Past Motion Encoder (PME) and the Future Motion Predictor (FMP) modules rely on attention mechanisms: SpatioTemporal Attention (ST-Attention) and Past Movement Guided Attention (PMG-Attention). These mechanisms are pivotal for capturing and integrating spatiotemporal dependencies in motion sequences.

**ST-Attention** ST-Attention combines temporal and spatial attention mechanisms to model joint relationships over time effectively. This attention mechanism is utilized within PME to encode past motion features.

The temporal attention mechanism operates on the sequence dependencies over time in the joint positions:

$$\mathbf{Q}^t, \mathbf{K}^t, \mathbf{V}^t = \mathcal{F}_{QKV}^t(\mathbf{H}^l) \quad (10)$$

$$\mathbf{Z}^t = \text{softmax} \left( \frac{(\mathbf{Q}^t (\mathbf{K}^t)^T)}{\sqrt{d_k}} \right) \mathbf{V}^t \quad (11)$$

where  $\mathbf{H}^l$  represents the input at the  $l^{th}$  layer,  $\mathbf{Q}^t, \mathbf{K}^t$ , and  $\mathbf{V}^t$  are queries, keys, and values, respectively, derived from  $\mathbf{H}^l$ , and  $d_k$  is the dimension of keys.

The spatial attention mechanism focuses on modeling joint relationships in space:

$$\mathbf{Q}^s, \mathbf{K}^s, \mathbf{V}^s = \mathcal{F}_{QKV}^s(\mathbf{Z}^t) \quad (12)$$

$$\mathbf{Z}^s = \text{softmax} \left( \frac{(\mathbf{Q}^s (\mathbf{K}^s)^T)}{\sqrt{d_k}} \right) \mathbf{V}^s \quad (13)$$

where  $\mathbf{Q}^s, \mathbf{K}^s$ , and  $\mathbf{V}^s$  are queries, keys, and values for spatial attention, respectively, similarly derived from  $\mathbf{Z}^t$ .  $\mathbf{Z}^s$  is the output of ST-Attention.

**PMG-Attention** PMG-Attention is employed within the Future Motion Predictor (FMP) module to incorporate past motion features into the prediction of future motion sequences. Unlike ST-Attention which focuses on the past motion sequence itself, PMG-Attention applies cross-attention between the current state and the past motion features:

$$\mathbf{Q}^t, \mathbf{K}^t, \mathbf{V}^t = \mathcal{F}_{QKV}^t(\mathbf{H}^l), \mathcal{F}_{QKV}^t(\mathbf{H}^P) \quad (14)$$

$$\mathbf{Z}^t = \text{softmax} \left( \frac{(\mathbf{Q}^t (\mathbf{K}^t)^T)}{\sqrt{d_k}} \right) \mathbf{V}^t \quad (15)$$

$$\mathbf{Q}^s, \mathbf{K}^s, \mathbf{V}^s = \mathcal{F}_{QKV}^s(\mathbf{Z}^t), \mathcal{F}_{QKV}^s(\mathbf{H}^P) \quad (16)$$

$$\mathbf{Z}^s = \text{softmax} \left( \frac{(\mathbf{Q}^s (\mathbf{K}^s)^T)}{\sqrt{d_k}} \right) \mathbf{V}^s \quad (17)$$

where  $\mathbf{Q}^t$  and  $\mathbf{Q}^s$  are obtained from the hidden state of future motions, and the  $\mathbf{K}^t, \mathbf{V}^t, \mathbf{K}^s, \mathbf{V}^s$  are obtained from the features of past motion.

### 8. Implementation Details

We deployed our network using an NVIDIA RTX4090 GPU (with PyTorch 2.0). For training, we set the batch size to 24 and utilized the Adam optimizer with an initial learning rate of 0.00005. To enhance convergence, we implemented a cosine annealing learning rate schedule. These training parameters were consistently applied across all datasets in our experiments. We ensured that the GPU memory usage remained below 6GB, enabling our network to be seamlessly deployed on various hardware platforms with ease.

### 9. Complete Results on Human3.6M

We provide the full results of comparisons on the Human3.6M dataset in Tab. 7 as a supplement to Tab. 1. Despite the simplicity of our network structure, we achieved the best results on most actions.

### 10. Ablation Study on Model Architecture

**Way of Fusing Past Motion and Future Motion** In the default setting, we use cross-attention to integrate features of past and future motions. We experimented with other fusion methods, with results shown in Tab. 8: A) Direct addition of features from past and future actions; B) Concatenation of both in the feature dimension, followed by a

Table 7. Comparisons of MPJPEs between our proposed method with other *state-of-the-art* methods for short-term prediction on Human3.6. We show the results across all actions such as walking and eating. The best results are highlighted in bold, and the second best results are underlined.

Motion	Walking				Eating				Smoking				Discussion				Direction			
Milliseconds	80	160	320	400	80	160	320	400	80	160	320	400	80	160	320	400	80	160	320	400
DMGNN[20]	17.3	30.7	54.6	65.2	11.0	21.4	36.2	43.9	9.0	17.6	32.1	40.3	17.3	34.8	61.0	69.8	13.1	24.6	64.7	81.9
MSR[7]	12.2	22.7	38.6	45.2	8.4	17.1	33.0	40.4	8.0	16.3	31.3	38.2	12.0	26.8	57.1	69.7	8.6	19.7	43.3	53.8
Mixer[2]	12.0	23.0	42.4	51.3	7.8	16.5	34.3	43.0	7.4	15.2	30.3	37.6	10.7	25.0	56.9	71.1	7.5	18.4	43.9	55.3
PGBIG[26]	10.2	19.8	34.5	40.3	7.0	15.1	30.6	38.1	6.6	14.1	28.2	34.7	10.0	23.8	53.6	66.7	7.2	17.6	40.9	51.5
SPGSN[24]	10.1	19.4	34.8	41.5	7.1	14.8	30.5	37.9	6.7	13.8	28.0	34.6	10.4	23.8	53.6	67.1	7.4	17.2	40.0	50.3
siMLPe[12]	11.9	19.3	31.9	36.9	10.2	16.5	30.7	37.3	10.4	16.4	29.7	35.9	12.7	25.3	55.1	68.1	11.0	19.4	41.6	52.1
DSTD-GC[10]	11.1	22.4	38.8	45.2	7.0	15.5	31.7	39.2	6.6	14.8	29.8	36.7	10.0	24.4	54.5	67.4	6.9	17.4	40.1	51.7
AuxFormer[41]	<u>8.9</u>	<u>16.9</u>	<b>30.1</b>	<b>36.1</b>	<u>6.4</u>	<u>14.0</u>	<b>28.8</b>	<b>35.9</b>	<u>5.7</u>	<u>11.4</u>	<u>22.1</u>	<u>27.9</u>	<u>8.6</u>	<u>18.8</u>	<u>38.8</u>	<u>49.2</u>	<u>6.8</u>	<u>17.0</u>	40.3	51.6
CIST-GCN[33]	11.8	23.4	40.5	46.5	6.7	14.8	29.8	36.8	7.3	15.6	31.0	38.0	10.2	23.7	52.3	65.3	7.3	18.1	43.6	55.3
Ours	<b>8.6</b>	<b>16.5</b>	<u>31.2</u>	37.7	<b>6.1</b>	<b>13.7</b>	<u>29.3</u>	<u>36.8</u>	<b>5.3</b>	<b>10.3</b>	<b>19.7</b>	<b>25.2</b>	<b>7.7</b>	<b>16.3</b>	<b>31.7</b>	<b>40.9</b>	<b>6.3</b>	<b>15.8</b>	<b>39.8</b>	<u>51.4</u>
Motion	Greeting				Phoning				Posing				Purchases				Sitting			
Milliseconds	80	160	320	400	80	160	320	400	80	160	320	400	80	160	320	400	80	160	320	400
DMGNN[20]	23.3	50.3	107.3	132.1	12.5	25.8	48.1	58.3	15.3	29.3	71.5	96.7	21.4	38.7	75.7	92.7	11.9	25.1	44.6	<b>50.2</b>
MSR[7]	16.5	37.0	77.3	93.4	10.1	20.7	41.5	51.3	12.8	29.4	67.0	85.0	14.8	32.4	66.1	79.6	10.5	22.0	46.3	57.8
Mixer[2]	16.4	37.1	80.2	98.2	9.1	19.5	42.4	53.6	11.5	27.0	64.9	83.5	13.4	30.7	65.6	80.0	9.8	20.9	45.6	57.3
PGBIG[26]	15.2	34.1	71.6	87.1	8.3	18.3	38.7	48.4	10.7	25.7	60.0	76.6	12.5	28.7	<u>60.1</u>	<u>73.3</u>	8.8	<u>19.2</u>	42.4	53.8
SPGSN[24]	14.6	32.6	70.6	86.4	8.7	18.3	38.7	48.5	10.7	25.3	59.9	76.5	12.7	28.6	61.0	74.4	9.3	<u>19.4</u>	<u>42.2</u>	53.6
siMLPe[12]	16.2	33.7	70.9	86.3	11.9	20.3	39.7	48.9	13.9	27.3	62.0	78.6	15.5	29.3	<b>59.3</b>	<b>72.0</b>	13.2	21.9	44.5	55.7
DSTD-GC[10]	14.3	33.5	72.2	87.3	8.5	19.2	40.3	49.9	10.1	25.4	60.6	77.3	12.7	29.7	62.3	75.8	8.8	19.3	42.9	54.3
AuxFormer[41]	<u>13.5</u>	31.3	69.2	85.4	<u>7.9</u>	<u>17.3</u>	<b>37.4</b>	<b>47.2</b>	<u>8.8</u>	<u>19.1</u>	<u>39.2</u>	<u>51.0</u>	<u>11.9</u>	<u>28.0</u>	61.8	76.3	<u>8.7</u>	<b>19.0</b>	<b>42.1</b>	53.3
CIST-GCN[33]	13.7	31.0	65.7	79.9	8.6	18.5	39.3	49.6	9.6	23.7	57.7	75.0	13.3	30.2	63.0	77.3	8.9	19.4	42.3	53.6
Ours	<b>10.8</b>	<b>26.4</b>	<b>62.7</b>	<b>79.8</b>	<b>7.5</b>	<b>17.1</b>	<u>37.9</u>	<u>48.0</u>	<b>8.2</b>	<b>16.9</b>	<b>32.8</b>	<b>43.5</b>	<b>11.4</b>	<b>27.6</b>	<u>62.6</u>	<u>77.6</u>	<b>8.5</b>	<u>19.2</u>	44.3	<u>56.7</u>
Motion	Sitting Down				Taking Photo				Waiting				Walking Dog				Walking Together			
Milliseconds	80	160	320	400	80	160	320	400	80	160	320	400	80	160	320	400	80	160	320	400
DMGNN[20]	15.0	32.9	77.1	90.3	13.6	29.0	46.0	58.8	12.2	24.2	59.6	77.5	47.1	93.3	160.1	171.2	14.3	26.7	50.1	63.2
MSR[7]	16.1	31.6	62.5	76.8	9.9	21.0	44.6	56.3	10.7	23.1	48.3	59.2	20.7	42.9	80.4	93.3	10.6	20.9	37.4	43.9
Mixer[2]	15.3	30.5	62.7	78.0	9.0	19.9	44.7	56.9	9.9	22.0	49.7	62.5	21.1	43.9	84.7	101.2	9.9	20.4	39.3	47.3
PGBIG[26]	13.9	27.9	57.4	71.5	8.4	18.9	42.0	53.3	8.9	20.1	43.6	54.3	<u>18.8</u>	<u>39.3</u>	<u>73.7</u>	86.4	8.7	18.6	34.4	41.0
SPGSN[24]	14.2	27.7	<u>56.7</u>	70.7	8.8	18.9	<u>41.5</u>	<u>52.7</u>	9.2	19.8	43.1	54.1	-	-	-	-	8.9	18.2	33.8	40.9
siMLPe[12]	18.0	29.8	57.7	71.2	13.1	21.3	42.9	53.6	11.9	21.5	44.4	55.0	21.8	40.6	74.6	87.0	11.9	19.8	34.2	39.8
DSTD-GC[10]	14.1	28.0	57.3	71.2	8.4	18.8	42.0	53.5	8.7	20.2	44.3	55.3	19.6	41.8	77.6	90.2	9.1	19.8	36.3	42.7
AuxFormer[41]	<u>13.5</u>	<u>27.6</u>	<b>57.7</b>	72.2	<u>8.2</u>	<u>18.4</u>	<u>41.5</u>	53.0	<u>8.2</u>	<u>18.5</u>	<b>41.2</b>	<b>52.2</b>	<b>17.1</b>	<b>36.5</b>	<b>70.4</b>	<b>83.0</b>	<u>7.8</u>	<u>15.9</u>	<b>30.2</b>	<b>37.0</b>
CIST-GCN[33]	14.1	29.8	57.3	<u>69.8</u>	<u>8.2</u>	<u>18.4</u>	<b>40.6</b>	<b>51.8</b>	8.6	19.4	43.5	54.8	20.0	41.4	<u>73.7</u>	<u>85.1</u>	9.6	20.3	38.2	45.6
Ours	<b>10.1</b>	<b>17.2</b>	<b>30.2</b>	<b>39.2</b>	<b>7.6</b>	<b>17.8</b>	42.0	54.1	<b>7.8</b>	<b>18.0</b>	<u>41.6</u>	<u>53.2</u>	19.1	41.1	80.6	95.2	<b>7.3</b>	<b>15.3</b>	30.8	37.9

Table 8. Ablation study of model architecture

ID		80ms	160ms	320ms	400ms
A	add	9.4	20.1	42.7	53.5
B	connect	9.2	20.1	42.7	53.7
C	parallel <i>attn.</i>	9.1	20.1	42.3	52.9
D	complete	<b>8.8</b>	<b>19.3</b>	<b>41.1</b>	<b>51.8</b>

Linear layer to reduce the number of channels back to the original value. We observed that cross-attention is the best choice because it explicitly computes the temporal and spatial interactions between the past and future motion.

Table 9. Impact of model size.  $d$  is the feature dimension.  $l$  is the number of layers.

ID		80ms	160ms	320ms	400ms	Param
E	$d = 64$	9.3	20.2	43.3	54.4	0.67M
F	$d = 128$	9.1	19.8	42.0	52.9	1.00M
G	$l = 2$	9.2	20.2	42.6	53.3	1.16M
H	$l = 4$	<b>8.8</b>	19.3	41.6	52.3	2.15M
D	complete	<b>8.8</b>	<b>19.3</b>	<b>41.1</b>	<b>51.8</b>	1.66M

**Spatiotemporal Attention** In the default setting, we follow the AuxFormer[41] of computing temporal and spatial attention sequentially. Results of parallel computation of

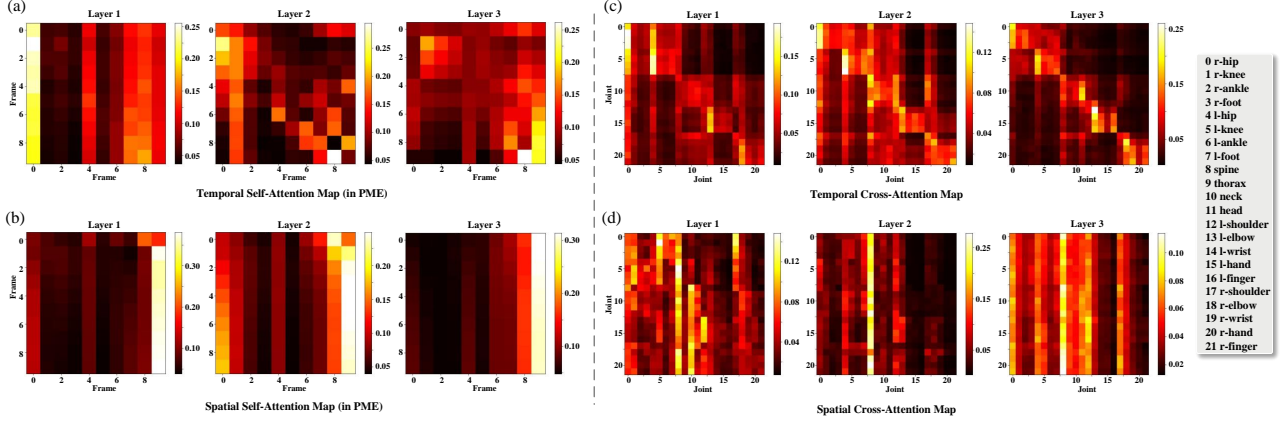


Figure 4. Visualization of attention feature maps.

temporal and spatial attention are presented in Tab. 8 C, showing worse performance.

**Model Size** In Tab. 9, we show the impact of different model sizes (including feature dimension  $d$  in attention layer and number of layers  $l$ ) on parameter count and results. Although reducing the model size can decrease the number of parameters, it can also lead to decreased performance. We observe that the default setting ( $d=256$ ,  $l=3$ ) represents the optimal balance between parameter count and performance.

## 11. Visualization of Attention Feature Map

For the example of the Discussion action, we present the averaged attention feature maps over 512 samples. As shown in Fig. 4, sub figure (a) and (b) display the temporal self-attention and spatial self-attention feature maps from different layers in PME, sub figure (c) and (d) show the temporal cross-attention and spatial cross-attention feature maps from different layers in FMP.

In temporal cross-attention, the model’s first and third layers tend to allocate attention to the later frames, as these frames have a greater influence on future sequences. In the second layer, the model distributes attention to both later and earlier frames, highlighting the potential impact of historical sequences on future actions. In spatial cross-attention, the model identifies significant correlations between the movement patterns of the ‘thorax’, ‘head’, ‘left elbow’, and ‘right elbow’ joints and the prediction of future actions.